Cognitive Computation (2025) 17:122
https://doi.org/10.1007/s12559-025-10478-2

RESEARCH

Handwriting-Based Gender Classification Using Robotic and Machine Learning Models

Belen Esther Aleman[1] · Moises Diaz[1] · Miguel A. Ferrer[1] · Jose Juan Quintana[1] · Marcos Faundez-Zanuy[2]

Received: 31 January 2025 / Accepted: 9 June 2025

Abstract

Handwriting analysis provides insights into motor control and cognitive processes, with potential differences arising from biological gender and neurological conditions such as Parkinson's disease (PD). Investigating these differences can lead to improved understanding of motor and cognitive functions. This study introduces a novel methodology that integrates robotic features to estimate gender from handwriting. Kinematic and dynamic features are estimated by simulating handwriting with a robotic model. Linear predictive coding (LPC) and singular spectrum analysis (SSA) are applied to the kinematic and dynamic sequences. Machine learning algorithms are used to classify handwriting as male or female. Handwriting samples from healthy individuals (BiosecurID database) and PD patients (PaHaW dataset) were analyzed. The proposed method demonstrates state-of-the-art performance in gender classification, revealing significant differences between healthy and unhealthy individuals. The robotic-based approach successfully mimics arm movements during writing, highlighting distinct motor patterns associated with gender and health status. This research advances the understanding of gender-based differences in motor and cognitive function, particularly in populations with neurological conditions. The integration of robotic features and machine learning provides a promising pathway for future investigations in handwriting analysis, gender classification, and neurodegenerative disease diagnosis.

Keywords Handwriting analysis · Gender classification · Machine learning

Introduction

Handwriting analysis has been widely studied in the field of biometrics, with one key objective being the identification of writer demographic characteristics. Research by Bouadjenek et al. [7] has demonstrated the feasibility of predicting gender from handwriting using feature extraction and machine learning techniques. Similarly, Asci et al. [4] used convolutional neural networks (CNNs) for age and gender classification, showcasing the potential of machine learning to detect subtle handwriting differences linked to the writer's gender.

The movement of the human arm shares significant similarities with a robotic chain composed of joints with varying degrees of freedom. When the end effector performs handwriting, the entire chain moves accordingly. However, current digitizers primarily capture the stylus trajectory and pressure, providing limited insight into the underlying arm movement or its physical properties, such as mass, inertia, and segment lengths.

This work is primarily a methodological study that focuses on both cognitive biometrics and neurodiagnostics. Through the integration of robotic modeling and machine learning techniques, we aim to explore the underlying movement characteristics associated with handwriting, assessing their relevance to individual identification and the detection of neuromotor pathologies.

In this study, we model a robotic arm to replicate handwriting tasks by estimating its kinematics and dynamics during the writing process. Robotics opens new avenues for biometric analysis and pattern recognition, as demonstrated in the development of robot kinematics for handwriting signature verification by Diaz et al. [14, 15]. Leveraging real kinematic and dynamic data from a UR5e robot and predicting these features using a multilayer perceptron have also shown promising results in the signature verification

✉ Belen Esther Aleman
belen.aleman103@alu.ulpgc.es

[1] Instituto Universitario para el Desarrollo Tecnológico y la Innovación en Comunicaciones (iDeTIC), Universidad de Las Palmas de Gran Canaria, Las Palmas de Gran Canaria, Spain

[2] Tecnocampus, Universitat Pompeu Fabra, 08302 Mataró, Spain

Published online: 19 June 2025

domain [16]. Despite these advancements, kinematic and dynamic features remain underexplored in the context of gender classification through handwriting. In this work, we apply machine learning models to analyze movement patterns, with the goal of accurately classifying the writer's gender based on distinctive motion characteristics.

An additional experimental novelty of this work lies in the examination of handwriting from both healthy individuals and those affected by Parkinson's disease (PD). Handwriting impairments are among the early motor symptoms of Parkinson's disease. By evaluating handwriting across both healthy and PD-affected individuals, we assess the robustness of robotic feature modeling in populations with motor deficits.

Our research presents an innovative method for gender classification through handwriting by integrating robotic modeling and machine learning techniques. By clearly defining the methodological focus and emphasizing neurodiagnostic applications, we provide a structured framework that advances both cognitive biometrics and PD-related research. The results suggest that combining robotics with advanced machine learning opens new pathways for research and practical applications, including individual identification and the detection of neuromotor pathologies.

Although handwriting traits are generally associated with biological sex, we follow the convention established in the literature by using the term "gender classification" throughout this work. This choice aligns with the labeling in the databases, where participants are categorized as "male" or "female" based on self-reported gender identity.

Handwriting and Cognitive Computation

The relationship between handwriting and cognitive computation has long been of interest to researchers seeking to understand the interplay between motor control and higher-order brain functions. Cognitive computation, a field that draws inspiration from how biological systems process, store, and use information, provides powerful tools for analyzing and interpreting complex patterns in handwriting. Handwriting tasks inherently involve both motor execution and cognitive planning, making them an ideal subject for exploring cognitive processes such as decision-making, memory retrieval, and sensory-motor integration.

The features extracted through singular spectrum analysis (SSA) and linear predictive coding (LPC) are not only statistical summaries but also reflect cognitive processes such as pattern decomposition, temporal prediction, and planning. SSA decomposes handwriting dynamics into dominant patterns, akin to the brain's decomposition of complex motor sequences into simpler sub-movements. LPC models the predictive aspect of motor behavior by estimating future states from past movements, resembling human anticipatory motor control strategies. Thus, the extracted features simulate core cognitive mechanisms underlying handwriting production.

Furthermore, integrating a robotic arm model enables a biomechanically grounded simulation of handwriting movement, offering insight into variability across populations, including individuals with Parkinson's disease. By combining these methodologies, the research aims to contribute to biometric analysis and the understanding of motor behavior in neurodegenerative conditions.

The article is structured as follows: the "Related Works" section reviews prior work on gender classification. The "Method" section details the methodology for estimating the kinematics and dynamics of the robotic arm. The "Experiments" section describes the experimental setup, databases, and classifiers used. The "Results" section presents experimental results, distinguishing between healthy and PD-affected handwriting. Finally, the "Conclusions" section concludes the paper with key findings and future directions.

Related Works

Gender classification through the use of machine learning has been an active area of research, with numerous studies providing different approaches and techniques to improve the accuracy and effectiveness of models.

Handwriting Image-Based Approaches

Study [7] explored the prediction of age, gender, and hand dominance from gradient features in handwriting. Their findings suggest that these features can capture relevant differences in handwriting patterns between genders. An automated method to predict age, gender, and nationality from handwriting in offline mode is presented in [1]. Using advanced image processing techniques, they demonstrated the effectiveness of these methods for accurate classifications. Investigating gender detection using written documents, AL-Qawasmeh and Suen [2] used transfer learning. This approach leverages pre-trained models to improve accuracy for handwriting tasks, showing significant improvements in gender classification. Next, Palaiahnakote et al. [31] developed a robust, script-independent system for gender identification from handwriting. This approach proved effective in gender classification regardless of language or writing style, demonstrating the versatility of their model.

Handwriting Kinematic-Based Approaches

In an approach focused on online handwriting, Marzinotto et al. [29] developed a two-layer clustering method to classify age and gender. This study revealed that dynamic features of handwriting can be valuable for gender identification,

showing promising results. On the other hand, Rabaev et al. [33] used a bilinear ResNet for automatic gender and age classification from offline handwriting. This method was noteworthy for its robustness and accuracy, demonstrating the capability of ResNet networks to extract discriminative features. The study in [36] explored gender recognition based on online handwriting using statistical and machine learning techniques. Their results showed that these techniques can capture dynamic features of handwriting indicative of the writer's gender. Study [11] focused on gender identification through online handwriting, using machine learning techniques to achieve high accuracy. This underlined the importance of temporal and dynamic features in handwriting for gender classification. Gender differences in online handwriting signals to improve e-Health and e-Safety applications were analyzed in [20]. Their findings highlighted the effectiveness of online handwriting features for gender classification. Study [35] investigated gender classification using online allographies. Their text-dependent allographic approach proved effective, highlighting the relevance of textual features in gender identification. Meanwhile, Maurer [30] examined differential patterns in early handwriting between girls and boys, finding significant differences that influence gender classification. This study highlighted the importance of considering gender differences from an early age [31].

Other Modalities

For this task of gender classification, the literature has used other modalities beyond handwriting. For example, in [26], the use of CNNs is proposed to classify a person's age and gender from facial images. The research showed that CNNs are capable of extracting robust features and performing accurate classifications, highlighting their effectiveness in gender identification. Facial images and voice were combined in [32] in a deep neural network model for combined age and gender classification. Using fine-tuning techniques, they were able to improve classification accuracy, highlighting the importance of integrating multiple data modalities. In a different approach, Russel and Selvaraj [34] investigated gender discrimination, age group classification, and carried object recognition using gait energy images and a fusion of parallel neural networks. This study showed how motion features can be useful for gender classification.

Method

Our work proposes estimating angular positions and torque during handwriting tasks. To achieve this, a linear position (x, y, z) of a handwriting sample registered through a digitizer is required. We then develop a robot with characteristics similar to a human arm to determine, by developing robotic kinematics, the angular positions $(\theta_1, \theta_2, \theta_3, \theta_4, \theta_5)$ that the robot's joints would adopt to reach that linear position. From the angular position, the dynamics of the robot have been worked out to calculate the torques $(\tau_1, \tau_2, \tau_3, \tau_4, \tau_5)$ of each joint. Figure 1 shows a diagram of the process described. The designed robot configuration is described in the "Robotic Configuration" section. The "Robot Kinematics" section explains the development of the robot kinematics. Finally, the "Robotic Dynamic Movement" section describes the developed dynamics of the robot.

Robotic Configuration

The robot model developed in this work aims to resemble the movement of the human arm, with the ability to execute the precise, complex movements a person makes when writing or drawing. This model is not based on a specific robot. Instead, physical and mathematical formulation was applied inspired by a human upper limb and ergonomic position to write. Figure 2a shows each link of the robot and its similarity to the human arm. The degrees of freedom (DoF) of the robot also aimed to mimic the DoF of human arms. The five DoF of our robotic model are highlighted in Fig. 2b.

To enhance the realism in the robot, anthropometric data on average forearm, hand, and finger lengths were obtained by reference to [5]. In addition to the length, the mass of each link was determined. This needed to consider the combined weight of the forearm and hand as representing approximately 2.3% of total body mass, with the hand alone accounting for 0.7% [28]. To determine the weight of the forearm, the total weight of the forearm-hand combination is calculated, and the weight corresponding to the hand is subtracted [28]. The index finger was also estimated to weigh around 0.01 kg, so this value is subtracted from the mass of the hand, considering that the mass of the other fingers is included in the total weight of the hand. Table 1 presents the mass and length values for each link.

Having established the robotic configuration, we proceed to model its kinematics by solving the direct and inverse positioning problems.

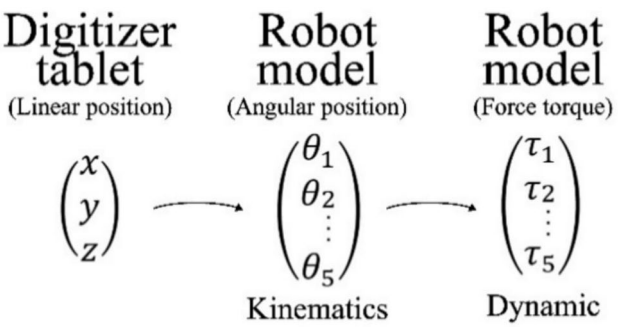

Fig. 1 Conversion of linear position to torque in robotic systems

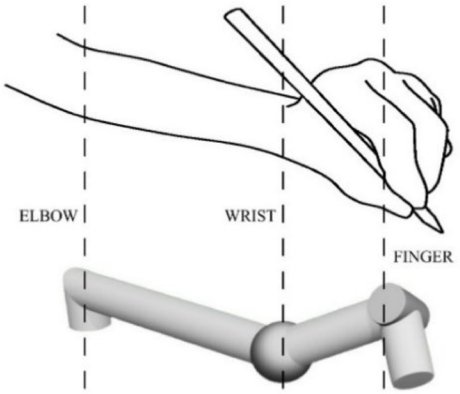

(a) Comparative study of human and robotic arm biomechanics.

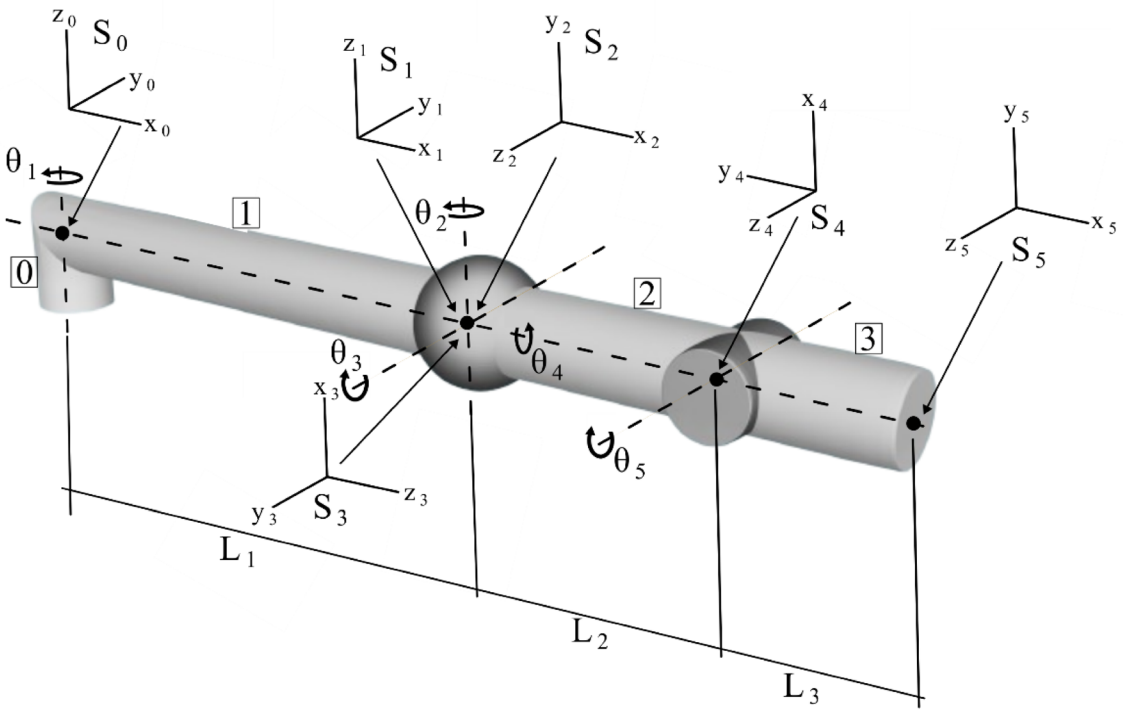

(b) Kinematic diagram of the 5-degree-of-freedom robotic arm with joint coordinates and reference frames.

Fig. 2 Conceptual model for the kinematic and biomechanical design of the robotic arm. **a** Comparative study of human and robotic arm biomechanics. **b** Kinematic diagram of the 5-degree-of-freedom robotic arm with joint coordinates and reference frames

Robot Kinematics

Robot kinematics aims to relate the changes in the position and orientation (pose) of the robot's end effector to the position of its joints $\theta = (\theta_1, \theta_2, \theta_3, \theta_4, \theta_5)$, without considering forces. The robot's end effector coordinates, $r = (r_x, r_y, r_z)$, are the only available information obtained from handwriting-based digitizers.

There are two main problems in the robot kinematics: on the one hand, studying the pose of the end effector based on the position of the kinematic chain joints, which has a unique solution, and on the other, calculating the position of the joints from the pose of the end effector. The solution to the latter is not usually unique and, if the system has more DoF than necessary, there may be infinite solutions.

Table 1 Mechanical dimensions of the links in the proposed robotic model [28]

Link	Length (cm)	Mass (kg)
L1	28	1.26
L2	11	0.48
L3	10	0.01

The calculation of a robot's end-effector pose related to the positions of its joints is commonly performed using the Denavit-Hartenberg algorithm [13], which is a widely used method in robotics. This algorithm assigns a reference frame to each joint and, by relating each frame to the previous one, enables the determination of the end-effector pose relative to the base frame. Figure 2b shows the reference frames associated with each DoF of our robotic model.

According to this method, each joint is fully defined by four parameters which are the movements to be performed in the reference system $\{S_{i-1}\}$ so that it coincides with the reference system $\{S_i\}$. In this context, $\{S_{i-1}\}$ represents the reference frame of the anterior joint, and $\{S_i\}$ represents the reference frame which describes the relative position and orientation of joint i. These parameters are the angle θ_i that must be rotated about the z_{i-1} axis so that the x_{i-1} and x_i axes are parallel, the displacement d_i that must be moved along the z_{i-1} axis so that the x_{i-1} and x_i axes are aligned, the displacement a_i that must be moved along the new x_{i-1} axis so that the two reference systems are in the same place, and finally the angle α_i that must be rotated about the new x_{i-1} axis so that the z_{i-1} and z_i axes coincide.

Applying this algorithm to the kinematic chain in Fig. 2b gives the Denavit-Hartenberg parameters in Table 2.

In Table 2, the row corresponding to joint i relates the reference system $\{S_i\}$ to the reference system $\{S_{i-1}\}$ by using the homogeneous transformation matrix ${}^{i}A_{i-1}$ [11], given by Eq. 1:

$$ {}^{i}A_{i-1} = \begin{pmatrix} \cos(\theta_i) & -\cos(\alpha_i)\sin(\theta_i) & \sin(\alpha_i)\sin(\theta_i) & a_i\cos(\theta_i) \\ \sin(\theta_i) & \cos(\alpha_i)\cos(\theta_i) & -\sin(\alpha_i)\cos(\theta_i) & a_i\sin(\theta_i) \\ 0 & \sin(\alpha_i) & \cos(\alpha_i) & d_i \\ 0 & 0 & 0 & 1 \end{pmatrix} \tag{1} $$

Because homogeneous transformation matrices can be composed, the one relating the robot end to its base can be calculated easily by means of Eq. 2 as follows:

Table 2 Denavit-Hartenberg parameters for the study robot [13]

Joint	θ	d	a	α
1	θ_1	0	L_1	0
2	θ_2	0	0	$\frac{\pi}{2}$
3	$\theta_3 + \frac{\pi}{2}$	0	0	$\frac{\pi}{2}$
4	θ_4	L_2	0	$\frac{-\pi}{2}$
5	$\theta_5 - \frac{\pi}{2}$	0	L_3	0

$$ {}^{0}A_5 = {}^{0}A_1\,{}^{1}A_2\,{}^{2}A_3\,{}^{3}A_4\,{}^{4}A_5 \tag{2} $$

where the first three rows of the last column of the matrix ${}^{0}A_5$ give the position of the end of the robot relative to the base reference system $\{S_0\}$. Therefore, the position of the end of the robot relative to its base can be known in this way, based on the angles θ_i.

Nevertheless, our aim is to calculate the joint positions given a specific end-effector position. It is important to note that since the robot has five DoF and only the position of the target point is known, equivalent to three DoF, two angles must be fixed to render the system solvable. These angles can be chosen freely to define, for instance, the hand orientation or other parameters.

The literature describes several methods for calculating robot angles [11]: trigonometric methods, iterative methods based on the homogeneous transformation matrix, and iterative methods based on Jacobians, among others. For this work, an iterative method based on the homogeneous transformation matrix was chosen as it is an immediate method if the D-H parameters of the robot are known and because the calculation time is not a critical factor for the handwriting tasks to be performed.

To implement this method, a function must be defined to minimize f_R. This function takes three input parameters: the spatial point r, used to compute the robot's angles; a set of five angles θ, which, according to Eq. 2, determine the position reached by the robot; and two additional angles that remain constant. The function's output parameter is the error, which is defined as the Euclidean distance between the desired point and the point reached by the robot with the given angles. If this error is less than a specified threshold (10^{-4} by default), the angles are considered a valid solution to the kinematic problem.

The procedure for calculating the angles is described as follows:

- Start with a point r located within the robot's working area, referred to the robot base coordinate frame, identified as $\{S_0\}$ in Fig. 2b.
- Define the two angles that will remain constant during the calculation.
- Select a seed, a set of three initial values for the iterations, to calculate the remaining three angles θ_s. A bank of seeds is available to cover all possible positions of the robot.
- Determine the desired angles using the Nelder-Mead simplex minimization algorithm [24], specifying the function to be minimized, f_R, and the seed chosen. The MATLAB fminsearch function, which implements this algorithm, is used for the calculation.
- If the minimization algorithm does not converge, repeat steps 3 and 4 with a new seed.

The redundancy in our robotic arm, modeled with five degrees of freedom (DoF), mirrors the redundancy inherent in the human upper limb, where multiple joint configurations can achieve identical end-effector positions. This characteristic parallels human motor control strategies where the central nervous system resolves multiple feasible movements by optimizing effort, stability, or sensory feedback, as described in muscle synergy theories. Modeling inverse kinematics thus serves not only mechanical purposes, but also provides a bioinspired approximation of human motor planning processes.

In this article, the angles θ_2 and θ_4 were set to 0° and 50°, respectively, to approximate typical wrist and hand configurations during handwriting tasks, as reported in ergonomic studies. A sensitivity analysis indicated that moderate variations of $\pm 10°$ around these values did not significantly impact the resulting torque or classification performances, supporting the robustness of this choice.

Robotic Dynamic Movement

Robot dynamic analysis focuses on how applied forces influence the motion of the robot. The dynamic model of a robot is derived from the values of the angular position $(\theta_1, \theta_2, \cdots \theta_5)$. For robots with one or two degrees of freedom, the solution is relatively straightforward. However, for robots with multiple degrees of freedom, the equations become considerably more complex, requiring the use of iterative methods to solve the dynamic equations [12].

To estimate the torques of each joint, an iterative method was used through the dynamics of the robot, specifically the Newton–Euler method. This method follows 10 steps in which it is possible to find the torque of each link. Subsequently, to simulate dynamic handwriting motions, we model the forces and torques involved using Newton–Euler formalism. In addition, depending on the configuration of the robot, this method presents equations for translational or rotational joints [12, 23]. According to the configuration of the joints presented in the study robot, the rotational equations were used. As we assume that the writer was at rest before writing, the initial angular velocity, angular acceleration, and linear velocity were zero, ${}^0\omega_0 = {}^0\dot{\omega}_0 = {}^0v_0 = [0,0,0]$.

The initial linear acceleration of the system, which depends on gravity, is described by Eq. 3, which includes the acceleration components due to gravity in the reference frame: g_{x0}, g_{y0}, and g_{z0}. In addition, a unit vector on the z-axis of the base reference frame, denoted as z_0 whose values are [0,0, 1], is used to describe the direction of the initial z-axis. This description is crucial to establishing the dynamic equations and the forces acting on the robot links. The Newton–Euler algorithm takes advantage of these unit vectors to calculate the forces and torques required to control the robot's motion.

$$ {}^0\dot{v}_0 = -\left[g_{x0}, g_{y0}, g_{z0}\right] \tag{3}$$

Equation 4 is the formula that relates system $\{S_{i-1}\}$ to $\{S_i\}$. It describes the position of the system $\{S_i\}$ relative to the previous system by the coordinates, where b_i is the distance on the x-axis, d_i is the distance on the z-axis, and α_i is the angle of rotation around the x-axis:

$$ {}^ip_i = \left[b_i, d_i \cdot \sin(\alpha_i), d_i\cos(\alpha_i)\right] \tag{4}$$

Equation 5 calculates the angular velocity of the system $\{S_i\}$ by combining the transformed angular velocity of the system $\{S_{i-1}\}$ and the contribution from the angular velocity of the joint. The notation $\dot{\theta}_i$ refers to the rate at which the joint position changes. ${}^iR_{i-1}$ corresponds to the rotation matrix for the current system $\{S_i\}$ with respect to the previous system $\{S_{i-1}\}$.

$$ {}^i\omega_i = {}^iR_{i-1}\left({}^{i-1}\omega_{i-1} + z_0\dot{\theta}_i\right) \tag{5}$$

Equation 6 determines the angular acceleration of system $\{S_i\}$. It includes the angular acceleration of the system $\{S_{i-1}\}$, the angular acceleration of the joint itself, and the cross-product term ${}^{i-1}\omega_{i-1} \times z_0\dot{\theta}_i$ which considers how the previous angular velocity affects the current system angular acceleration. The notation $\ddot{\theta}_i$ refers to the angular acceleration of the joint.

$$ {}^i\dot{\omega}_i = {}^iR_{i-1}\left({}^{i-1}\omega_{i-1} + z_0\ddot{\theta}_i\right) + {}^{i-1}\omega_{i-1} \times z_0\dot{\theta}_i \tag{6}$$

Equation 7 calculates the linear acceleration of system $\{S_i\}$. Equation 9 determines the linear acceleration at the center of gravity of system $\{S_i\}$. Additionally, ${}^is_i$ represents the position vector of the center of mass of link i with respect to the coordinate system $\{S_i\}$.

$$ {}^i\dot{v}_i = {}^i\dot{\omega}_i \times {}^ip_i + {}^i\omega_i \times \left({}^i\omega_i * {}^ip_i\right) + {}^iR_{i-1}\,{}^{i-1}\dot{v}_{i-1} \tag{7}$$

$$ {}^ia_i = {}^i\dot{\omega}_i \times {}^is_i + {}^i\omega_i \times \langle {}^i\dot{\omega} | i * {}^is_i\rangle + {}^i\dot{v}_i \tag{8}$$

To reach this last step, the Newton–Euler algorithm requires calculation of the force of each link according to Eq. 10. This equation is used to determine the force in a link ${}^if_i$ by calculating, in the force of the subsequent link ${}^{i+1}f_{i+1}$, an initial external force and the acceleration of the current link ${}^ia_i$. The mass m_i is the mass of the system that corresponds to the link to which it belongs, thus providing an accurate representation of how forces and accelerations

interact within the moving system. That is, Eq. 10 first requires an external force and then depends on the force of the upper reference frame:

$$^{i}f_{i} = {}^{i}R_{i+1}{}^{i+1}f_{i+1} + m_{i}{}^{i}a_{i} \tag{9}$$

To calculate the first external pressure, in our case corresponding to ${}^{6}pr_{6}$, Eq. 11 is used. This equation, [19], converts the pressure measured on the ink tool into a force. This conversion is required because the databases used contain data on pressure on the writing surface.

$$\begin{aligned} pressure\left({}^{6}pr_{6}\right) = {} & 5.48 \cdot 10^{-6} \cdot \left({}^{6}pr_{6}\right)^{6} + 3 \cdot 10^{-3} \cdot \left({}^{6}pr_{6}\right)^{5} - 0.13 \cdot \left({}^{6}pr_{6}\right)^{4} \\ & -0.76 \cdot \left({}^{6}pr_{6}\right)^{3} + 6.52 \cdot \left({}^{6}pr_{6}\right)^{2} + 28.89 \cdot \left({}^{6}pr_{6}\right) - 9.90 \end{aligned} \tag{10}$$

The solution of the sixth-degree polynomial was obtained with MATLAB, which uses numerical methods to find the solution. The pressure values are converted into units in the international system of units (SI) to obtain the force of the last link ${}^{6}f_{6}$. Equation 12 has been used for this, where the area used in the formula is 0.08, corresponding to the surface area of the pen [19].

$$Force\left({}^{6}f_{6}\right) = pressure\left({}^{6}pr_{6}\right) \cdot area \tag{11}$$

Equation 13 shows the equation for the exerted torque. The first calculation requires an external torque, which in this case is 0, and then depends on the calculated torque of the upper link. Furthermore, this equation uses the matrix which corresponds to the inertia matrix. In our case, the inertia matrix for each $\{S_i\}$ is a 3×3 matrix with all its elements equal to 0, because the center of mass coincides with the center of gravity. This means there are no moments of inertia about the reference axes, thus simplifying the calculations.

$$\begin{aligned} {}^{i}n_{i} = {} & {}^{i}R_{i+1}\left[{}^{i+1}n_{i+1} + \left({}^{i}R_{i+1}{}^{i}p_{i}\right) \times {}^{i+1}f_{i+1}\right] \\ & + \left({}^{i}p_{i} + {}^{i}s_{i}\right) \times m_{i}{}^{i}a_{i} + {}^{i}I_{i}{}^{i}\omega_{i} + {}^{i}\omega_{i} \times \left({}^{i}I_{i}{}^{i}\omega_{i}\right) \end{aligned} \tag{12}$$

In Eq. 14, the general Newton–Euler formula that describes the torque of a rotational joint is shown, corresponding to the last step of the algorithm.

$$\tau_{i} = {}^{i}n_{i}{}^{i}R_{i-1}z_{0} \tag{13}$$

In addition, in the databases, the position on the z axis is recorded as movements in the air and on the surface, represented with the values of 0 and 1, respectively. For this purpose, it was established that for the value 0, the z axis would correspond to 4 mm, which is a reasonable pen-up distance with respect to the table.

Experiments

Databases

In this study, we used two databases that provide handwriting of individuals selected by gender. On the one hand, we used the BiosecurID database [21], which includes different handwriting-based tasks executed by healthy males and females. On the other hand, we used the PaHaW database [17, 18], which includes other handwriting tasks differentiated by gender. This database also contains handwriting carried out by healthy individuals and people affected by Parkinson's disease. These two corpuses enabled us to test the robustness of our robotic features on different handwriting tasks produced by healthy and unhealthy individuals by gender.

BiosecurID Database

The "Biometric Multimodal Database" [21] acquired within the BiosecurID project (BiosecurID) is a common database used in the analysis of gender classification through handwriting [20, 35], since it includes several biometric traits in addition to handwriting tasks. In total, 400 healthy participants (215 (53.75%) males and 185 (46.25%) females) with a mean age of 31.94 (SD of 12.49) were involved in the data collection. For the handwriting tasks, they used an inking pen and a Wacom Intuos3 A4 digitizer, which was set up at 5080 dpi, 1024 pressure levels, and an accuracy of around 0.25 mm. All handwriting tasks were studied in this article, which were repeated four times in four sessions over a time span of 4 months: (1) 1×4 digit sequence from 1 to 9 and the last the 0 (HW1); 1×4 upper-case words, 16 words per handwriting task (HW2); 1×4 Spanish text in lower-case (HW3); 3×4 genuine signatures (SG); and 3×4 skilled forgery signatures (FAKE SG).

PaHaW Database

The "Parkinson's disease handwriting database" (PaHaW) includes 38 healthy writers (20 (52.63%) males and 18 (47.37%) females) and 37 affected by Parkinson's disease (19 (51.35%) males and 18 (48.65%) females). Both healthy (mean age of 62.4 and SD of 11.3) and unhealthy (mean age of 69.3 and SD of 10.9) volunteers executed eight handwriting-based tasks contained in an unfilled template and holding an inking pen over a Wacom Intuos 4 M digitizer [17, 18]. The following eight handwriting tasks were required to be completed by all participants in

a single section: (1) drawing an Archimedes spiral (SPIRAL); (2) writing in cursive the letter (l); (3) the bigram le (le); (4) the trigram les (les); (5) writing in cursive the word "female teacher" in Czech (WORD 1); (6) writing in cursive the word "to compare" in Czech (WORD 2); (7) writing in cursive the word "to not catch" in Czech (WORD 3); and writing in cursive the sentence "The tram won't go today" in Czech (SENT).

Classifiers and Settings

With the purpose of distinguishing between handwriting samples according to the gender of healthy and unhealthy people, we compared different machine learning methods to identify differences between these groups. The main objective of this was to compare the machine learning methods in classifying handwriting by gender. For this, SVM, NN, and CNN learning machines were used, considering the analysis as a binary classification.

The support-vector machine (SVM) is a machine learning algorithm that analyzes data to classify and predict outcomes. SVMs can perform linear and non-linear classifications, using methods that transform data into a complex feature space, drawing boundaries between two sets of data to minimize classification errors [27].

Neural networks (NN) are a machine learning model determined by a layered structure that simulates the neural connections of the human brain. This configuration allows them to determine decisions through the simulation of neural processes [9]. This facilitates learning from data to identify patterns, organize information, and make predictions [27].

A convolutional neural network (CNN) is a deep machine learning network type that excels in image data processing. CNNs are organized into convolutional, pooling, and fully connected (FC) layers. Convolutional layers extract hierarchical features from the input data, while pooling layers perform spatial downsampling to reduce dimensionality and computational load. Additional components such as normalization and dropout layers are often included to improve training stability and prevent overfitting, and the fully connected layers integrate the extracted features for final classification [3].

As these classifiers require a fixed length input, the temporal sequences of the kinematic and dynamic values were transformed into fixed sequences using the linear predictive coding (LPC) and singular spectrum analysis (SSA) features. The LPC technique enables prediction of the future values of a signal from its previous values [8, 37], its main function being to represent the envelope of the signal spectrum using a parametric model [8]. In this context, h_i is the continuous signal h sampled at discrete time points, becoming a time series, and r_i, representing the estimation of h_i, is calculated as the weighted sum of n prior samples of h, where, $h_i \approx r_i = \sum_{j=1}^{n} t_j h_{i-j}$. Here, n is the model order, which determines the number of prior samples to be used in the estimation. The predictor coefficients $t_1,\ldots,t_n$ are adjusted such that they minimize the squared error [37], which is the sum of the squared differences between the actual values of the signal h_i and its estimates r_i over the time series, $\sum_i \left[h_i - r_i\right]^2$.

SSA is a technique used in temporal sequences with applications in signal processing and multivariate statistics, among other fields. The SSA methodology follows two phases, the first one individually decomposes the sequence, and the second uses these values to find the new components of the sequence [22]. In the study, the velocity subsignal was decomposed into 10 channels, the combination of which reproduces the original velocity signal, v_f. Ten channels are used because they allow detailed decomposition of the signal, facilitating the analysis of the different energy components of the original signal. The velocity energy features are calculated by the fraction of energy contained in each channel.

$$v_f = \Delta(f) \tag{14}$$

$$S_{fn} \leftarrow SSA\left(v_f, N\right); n = 1,, 2, ..., N = 10 \tag{15}$$

$$F_{fn} = \frac{\Sigma_{l=0}^{l_{SSA}} \left|S_{fn}\right|}{f_{te}} \tag{16}$$

$$f_{te} = \sum_{n=1}^{N=10} \sum_{l=0}^{l_{SSA}} \left|S_{fn}\right| \tag{17}$$

Initially, the velocity subsignals are calculated using Eq. 14. The velocity is divided by SSA, which takes v_f as input and splits it into 10 channels, giving rise to SSA channels (S_{fn}) as shown in Eq. 15. Sx1 represents the first channel obtained from the SSA assessment for trace x. Finally, the absolute energy of the SSA channels is scaled as a function of the total energy of the channels, obtaining the SSA characteristics shown in Eq. 16. In Eqs. 16 and 17, l_{SSA} is the upper limit of the sum, which indicates the total number of components or channels resulting from the SSA analysis, and $l = 0$ is the index indicating that the sum starts at 0 and continues until l_{SSA}.

Classification ability is evaluated with accuracy (ACC) and area under the curve (AUC) metrics.

$$ACC = \frac{TP + TN}{TP + TN + FP + FN} \cdot 100\% \tag{18}$$

$$AUC = \int_0^1 f(x)dx \tag{19}$$

In Eq. 18, the true positive (TP) indicates the number of people of one gender correctly identified and the false positive (FP) corresponds to the number of people classified as one gender who actually correspond to the other evaluation group. The true negative (TN) is the total number of people of one gender correctly identified and the false negative (FN) corresponds to the people of one gender who were labeled as if they were of the other gender to be evaluated. The AUC is a measure that evaluates the overall performance of a classification model, providing its effectiveness at all decision thresholds. Equation 19 presents the AUC formula, where (x) represents the function of the receiver operating characteristic (ROC) curve. The AUC ranges from 0 to 1, with 1 indicating a perfect classification model and 0.5 representing random performance [6, 25].

In the study, the position coordinates of the handwriting tasks were extracted from the databases to later reproduce them in the robot, where the values of the angles made in the execution of the handwriting tasks were obtained by means of the developed inverse kinematics algorithms. These values, together with the force exerted in each handwriting task, were extracted from the moment values using the dynamic problem. After obtaining the time sequences, it was decided to convert them into 12 values for the LPC coefficients and into 42 values for SSA. The choice of 12 values for the LPC coefficients was made to optimize the representation of the time sequences, since LPC enables prediction of the future values of a signal from its previous values, representing the envelope of the signal spectrum efficiently with a parametric model [37]. In the case of SSA, the transformation into 42 values allows for decomposition of the time series into principal components, capturing the most relevant trends and patterns in the data. The models were then trained by importing all the available samples, while reserving one of them for testing.

In addition, the "Leave-One-Out" (LOO) cross-validation method was used to train the machine learning machines used. This cross-validation technique, using a single data point as a test set and the rest of the data as a training set, enables a robust, detailed evaluation of model performance. Reference [9] demonstrated how LOO validation can be applied quickly and accurately on support vector machines with sparse least squares, thus optimizing the accuracy and efficiency of the model. On the other hand, Vehtari et al. [38] explored the effectiveness of LOO in evaluating Bayesian models, highlighting its ability to provide accurate estimates of the predictive capacity of models. The use of LOO in this study ensures that the models are able to generalize adequately to new data, improving the reliability of the results obtained.

Figure 3 shows the full pipeline of our work. First, the handwriting is digitalized and the tuple of trajectory and pressure is acquired (x,y,p). Then, we extract temporal robotic features based on a robot model. Specifically, we extract kinematic and dynamic features. Fixed numbers of features were explored by using SSA and LPC techniques. Finally, SVM, NN, and CNN machine learning experiments were carried out for gender classification.

Results

In the analysis of handwriting by gender, the objective of using the two databases was to evaluate the robustness of the robotic-based model characteristics in scenarios with healthy and unhealthy people. The results show a difference in discrimination by gender, as PD effects on handwriting can mask the gender characteristics. The results of analyzing healthy people's handwriting by gender are shown first, then the results of analyzing unhealthy people's handwriting by gender. The LPC and SSA characteristics for the two cases are shown in the "Gender Classification in Healthy People" section and in the "Analysis of Handwriting in Unhealthy People" section, where the best results are obtained.

Gender Classification in Healthy People

Tables 3 and 4 show the results of the LPC and SSA features, respectively, for the kinematic values of movement during

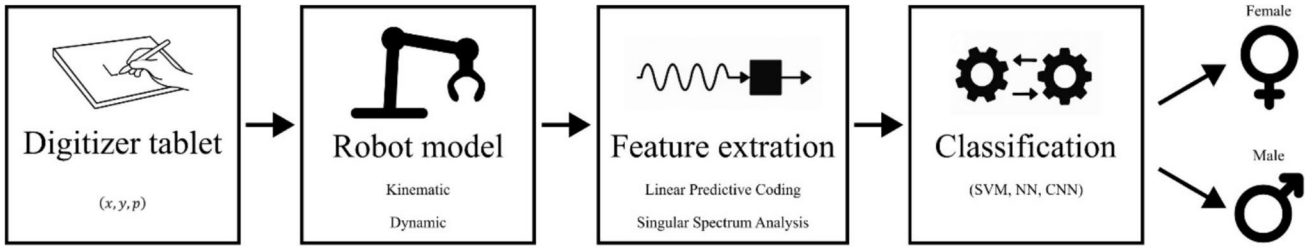

Fig. 3 Overview of the proposed methodology pipeline, illustrating the main stages from data acquisition, timing robotic features (kinematic and dynamic) in addition to SSA and LPC and classification stage using SVM, NN, and CNN classifiers

handwriting, i.e., $(\theta_1, \theta_2, \theta_3, \theta_4, \theta_5)$. Tables 5 and 6 show the results of the LPC and SSA features, respectively, for the dynamic values of movement, i.e., $(\tau_1, \tau_2, \tau_3, \tau_4, \tau_5)$. Finally, Tables 7 and 8 show the results of the LPC and SSA characteristics, respectively, for the combination of the kinematic-dynamic values of movement. The previous tables contain the results of the different handwriting tasks that include the BiosecurID databases and the PaHaW database.

The results in Table 3 show that, for the kinematic values, the BiosecurID database obtained the best classification result for the LPC features in the "SG" task (ACC = 61.19%; AUC = 66.61%) in the SVM and NN machine learning. However, for this database, the best classification is obtained in the SSA features in the same task (ACC = 68.19%; AUC = 74.34%) for the NN machine learning.

In the PaHaW database, it is observed that, for the LPC features, the SVM machine learning gives the best classification for the "SENT" task (ACC = 81.58%; AUC = 92.78%). For the SSA features, the same machine learning achieves the best classification. However, in this case, the corresponding task is "l" (ACC = 76.32%; AUC = 89.44%).

The BiosecurID database provides results for the dynamic values showing that, for the LPC features, the "SG" task obtains the best classification with the SVM machine learning (ACC = 63.81%; AUC = 67.59%). For the SSA features, the best classification is again obtained with the same task and machine learning (ACC = 65.38%; AUC = 68.89%).

The results obtained with the PaHaW database for the LPC features show that the "les" task (ACC = 76.32%; AUC = 75.28%) obtained the highest classification rate for the SVM machine learning. However, in the SSA features the best classification rate was obtained for the NN machine learning in the "l" task (ACC = 71.05%; AUC = 67.78%).

Table 3 Classification accuracy (ACC) and area under the curve (AUC) for LPC-derived kinematic features in healthy handwriting samples using SVM, NN, and CNN classifiers

Database	Handwriting task	SVM		NN		CNN	
		ACC	AUC	ACC	AUC	ACC	AUC
BiosecurID	HW1	55.58%	56.10%	53.30%	57.57%	51.02%	47.67%
	HW2	50.75%	50.09%	50.50%	52.42%	46.75%	49.59%
	HW3	55.08%	55.45%	53.30%	53.82%	59.14%	59.22%
	SG	61.19%	66.61%	61.19%	64.80%	50.06%	51.08%
	SG FAKE	53.51%	50.73%	50.58%	48.61%	51.42%	50.60%
PaHaW	SPIRAL	50.00%	44.89%	25.00%	30.96%	52.78%	49.23%
	l	65.79%	71.67%	63.16%	62.78%	50.00%	46.94%
	le	52.63%	49.17%	52.63%	53.61%	57.89%	56.11%
	les	50.00%	46.11%	55.26%	52.78%	50.00%	51.39%
	WORD 1	55.26%	64.72%	50.00%	54.17%	50.00%	45.56%
	WORD 2	65.79%	68.61%	44.74%	64.44%	50.00%	47.78%
	WORD 3	60.53%	64.17%	57.89%	66.11%	39.47%	32.22%
	SENT	81.58%	92.78%	55.28%	61.39%	52.63%	48.61%

Table 4 Classification accuracy (ACC) and area under the curve (AUC) for SSA-derived kinematic features in healthy handwriting samples using SVM, NN, and CNN classifiers

Database	Handwriting task	SVM		NN		CNN	
		ACC	AUC	ACC	AUC	ACC	AUC
BiosecurID	HW1	59.90%	65.40%	55.58%	58.14%	46.95%	43.24%
	HW2	58.75%	59.22%	52.00%	52.19%	48.75%	46.38%
	HW3	66.24%	71.44%	58.88%	62.23%	47.97%	45.04%
	SG	67.44%	70.16%	68.19%	74.34%	51.69%	51.92%
	SG FAKE	57.01%	59.70%	53.59%	54.20%	50.25%	50.91%
PaHaW	SPIRAL	47.22%	37.77%	44.44%	40.25%	47.22%	51.39%
	l	76.32%	89.44%	68.42%	79.72%	50.00%	46.94%
	le	63.16%	67.78%	52.63%	49.72%	44.74%	51.67%
	les	52.63%	56.39%	57.89%	61.39%	63.16%	68.65%
	WORD 1	63.16%	63.89%	52.63%	52.78%	39.47%	38.89%
	WORD 2	60.53%	60.83%	57.89%	56.11%	50.00%	53.91%
	WORD 3	47.37%	44.44%	60.53%	65.00%	42.11%	37.78%
	SENT	50.00%	58.33%	42.11%	39.72%	44.74%	47.78%

Table 5 Classification accuracy (ACC) and area under the curve (AUC) for LPC-derived dynamic features in healthy handwriting samples using SVM, NN, and CNN classifiers

Database	Handwriting task	SVM		NN		CNN	
		ACC	AUC	ACC	AUC	ACC	AUC
BiosecurID	HW1	58.12%	59.54%	58.38%	58.81%	53.55%	54.02%
	HW2	60.50%	64.58%	61.25%	67.22%	48.25%	46.17%
	HW3	49.24%	51.83%	49.75%	50.68%	49.24%	48.84%
	SG	63.81%	67.59%	59.81%	62.91%	52.38%	53.29%
	SG FAKE	53.17%	55.72%	54.34%	54.82%	51.25%	50.23%
PaHaW	SPIRAL	50.00%	50.77%	52.78%	52.63%	50.00%	52.32%
	l	50.00%	50.56%	52.63%	59.72%	55.26%	58.06%
	le	60.53%	52.50%	47.37%	48.61%	50.00%	50.00%
	les	76.32%	75.28%	52.63%	60.00%	42.11%	42.22%
	WORD 1	39.47%	48.61%	42.11%	42.78%	52.63%	60.00%
	WORD 2	73.68%	82.22%	36.84%	44.44%	50.00%	41.94%
	WORD 3	55.26%	55.83%	55.26%	58.06%	42.11%	46.11%
	SENT	71.05%	76.67%	57.89%	71.11%	57.89%	60.83%

Table 6 Classification accuracy (ACC) and area under the curve (AUC) for SSA-derived dynamic features in healthy handwriting samples using SVM, NN, and CNN classifiers

Database	Handwriting task	SVM		NN		CNN	
		ACC	AUC	ACC	AUC	ACC	AUC
BiosecurID	HW1	57.11%	59.36%	54.31%	57.55%	54.31%	55.69%
	HW2	57.50%	61.62%	54.75%	57.90%	53.50%	52.02%
	HW3	56.85%	60.59%	56.85%	61.06%	55.08%	52.75%
	SG	65.38%	68.89%	65.06%	70.90%	51.19%	50.08%
	SG FAKE	57.10%	58.49%	53.42%	55.45%	48.91%	47.17%
PaHaW	SPIRAL	61.11%	55.42%	44.44%	48.61%	38.89%	39.94%
	l	47.37%	50.56%	71.05%	67.78%	47.37%	50.28%
	le	65.79%	78.33%	60.53%	72.78%	47.37%	34.72%
	les	63.16%	60.83%	26.32%	30.28%	47.37%	45.00%
	WORD 1	60.53%	68.61%	71.05%	84.44%	44.74%	35.56%
	WORD 2	68.42%	71.94%	47.37%	54.44%	50.00%	52.22%
	WORD 3	55.26%	56.39%	52.63%	51.39%	52.63%	49.72%
	SENT	65.79%	72.87%	50.00%	48.06%	55.26%	51.94%

Table 7 Classification accuracy (ACC) and area under the curve (AUC) for LPC-derived kinematic-dynamic features in healthy handwriting samples using SVM, NN, and CNN classifiers

Database	Handwriting task	SVM		NN		CNN	
		ACC	AUC	ACC	AUC	ACC	AUC
BiosecurID	HW1	62.44%	64.54%	54.06%	55.84%	58.98%	48.08%
	HW2	59.00%	60.17%	56.75%	58.41%	49.00%	45.27%
	HW3	55.84%	55.80%	52.79%	53.46%	54.57%	55.35%
	SG	63.75%	68.65%	61.25%	65.59%	49.31%	49.20%
	SG FAKE	54.59%	55.51%	52.50%	50.90%	49.08%	49.93%
PaHaW	SPIRAL	47.22%	38.70%	33.33%	28.17%	33.33%	25.70%
	l	52.63%	64.72%	57.89%	61.11%	47.37%	48.61%
	le	50.00%	45.28%	52.63%	47.78%	50.00%	46.94%
	les	55.26%	66.67%	52.63%	53.61%	57.89%	50.00%
	WORD 1	63.16%	63.06%	52.63%	62.50%	47.37%	41.39%
	WORD 2	73.68%	80.00%	63.16%	55.56%	52.63%	51.67%
	WORD 3	65.79%	71.11%	65.79%	58.89%	31.58%	30.00%
	SENT	65.79%	78.89%	78.95%	80.83%	50.00%	44.72%

Table 8 Classification accuracy (ACC) and area under the curve (AUC) for SSA-derived kinematic-dynamic features in healthy handwriting samples using SVM, NN, and CNN classifiers

Database	Handwriting task	SVM		NN		CNN	
		ACC	AUC	ACC	AUC	ACC	AUC
BiosecurID	HW1	64.47%	68.44%	58.38%	60.48%	50.25%	49.68%
	HW2	59.75%	64.00%	55.50%	59.06%	51.75%	49.11%
	HW3	58.12%	64.39%	60.66%	63.85%	48.22%	46.45%
	SG	67.94%	72.88%	67.81%	73.59%	46.00%	43.25%
	SG FAKE	56.76%	58.31%	55.09%	57.26%	49.75%	49.41%
PaHaW	SPIRAL	50.00%	50.15%	47.22%	34.98%	41.67%	31.89%
	l	76.32%	82.50%	60.53%	62.50%	44.74%	48.89%
	le	65.79%	75.56%	55.26%	68.89%	44.74%	42.89%
	les	73.68%	73.33%	52.63%	53.61%	52.63%	51.39%
	WORD 1	71.05%	72.22%	52.63%	62.50%	55.26%	58.06%
	WORD 2	63.16%	63.33%	63.16%	55.56%	50.00%	53.33%
	WORD 3	55.26%	51.67%	65.79%	58.89%	50.00%	42.50%
	SENT	65.79%	55.28%	78.95%	80.83%	50.00%	57.50%

The results of the BiosecurID database obtained the best classification in the "SG" task with the SVM machine learning (ACC = 63.75%; AUC = 68.65%) for the LPC features in Table 7. However, this database achieved the highest classification value for the SSA feature (ACC = 67.94%; AUC = 72.88%) in Table 8.

The PaHaW database in the result of LPC features (Table 7) achieved the highest classification in the "SENT" task with the NN machine learning (ACC = 78.95%; AUC = 80.83%). In SSA features results (Table 8), the ACC value of 78.95% and AUC value of 80.83% was achieved in the "SENT" task with the same machine learning.

The different results show that, for the BiosecurID database, the SSA coefficients of the kinematics in Table 4 obtained the highest classification rate in the "SG" task in the NN machine learning (ACC = 68.19%; AUC = 74.34%). However, it is noted that the best results for the different cases are obtained in the "SG" task, but the "SG FAKE" task gave a low value. In the PaHaW database, the highest classification rate was obtained in the LPC features of the kinematics for the "SENT" task and the SVM machine learning (ACC = 81.58%; AUC = 92.78%). The "SPIRAL" task had notably low performance values.

Analysis of Handwriting in Unhealthy People

Table 9 shows the results of the LPC coefficients for the kinematic values of movement. Table 10 reflects the dynamic values for the LPC coefficients, and Table 11 shows the combination of the kinematic-dynamic values.

The results show that, for the kinematic values, the best classification rate was obtained in the "SENT" task with the NN machine learning (ACC = 75.68%; AUC = 78.36%) with the LPC features. For the dynamics, the best values are obtained for the "SPIRAL" task in the SVM machine learning (ACC = 75.00%; AUC = 70.37%) for the LPC features. Finally, for the combination of kinematics-dynamics, the "SPIRAL" task together with the SVM machine learning achieved the best classification rate (ACC = 72.22%; AUC = 65.12%) for the SSA features.

The best classification results obtained in the PaHaW database with movement of healthy and unhealthy people

Table 9 Classification accuracy (ACC) and area under the curve (AUC) for LPC-derived kinematic features in unhealthy handwriting samples using SVM, NN, and CNN classifiers

Database	Handwriting task	SVM		NN		CNN	
		ACC	AUC	ACC	AUC	ACC	AUC
PaHaW	SPIRAL	55.56%	51.54%	36.11%	37.35%	41.67%	42.28%
	l	43.24%	41.81%	40.54%	43.57%	48.65%	53.22%
	le	51.35%	52.92%	37.84%	53.51%	56.76%	66.08%
	les	48.65%	48.54%	40.54%	38.01%	48.56%	47.95%
	WORD 1	32.43%	28.65%	40.54%	39.47%	48.65%	49.42%
	WORD 2	56.76%	57.89%	45.95%	50.88%	37.84%	34.21%
	WORD 3	59.46%	61.99%	59.46%	58.77%	45.95%	49.71%
	SENT	67.57%	73.39%	75.68%	78.36%	43.24%	40.06%

Table 10 Classification accuracy (ACC) and area under the curve (AUC) for LPC-derived dynamic features in unhealthy handwriting samples using SVM, NN, and CNN classifiers

Database	Handwriting task	SVM		NN		CNN	
		ACC	AUC	ACC	AUC	ACC	AUC
PaHaW	SPIRAL	75.00%	70.37%	41.67%	52.47%	58.33%	56.17%
	l	51.35%	50.58%	54.05%	52.92%	45.95%	49.42%
	le	37.84%	38.01%	45.95%	37.13%	59.46%	52.05%
	les	64.86%	67.54%	35.14%	41.25%	37.84%	38.30%
	WORD 1	59.46%	71.05%	45.95%	57.02%	51.35%	46.20%
	WORD 2	64.86%	64.04%	59.46%	62.28%	43.24%	48.54%
	WORD 3	64.86%	69.59%	48.65%	41.81%	37.84%	36.84%
	SENT	54.05%	53.51%	48.65%	50.29%	51.35%	56.14%

Table 11 Classification accuracy (ACC) and area under the curve (AUC) for SSA-derived kinematic-dynamic features in unhealthy handwriting samples using SVM, NN, and CNN classifiers

Database	Handwriting task	SVM		NN		CNN	
		ACC	AUC	ACC	AUC	ACC	AUC
PaHaW	SPIRAL	72.22%	65.12%	63.89%	65.43%	41.67%	49.38%
	l	59.46%	62.28%	54.05%	58.19%	48.65%	41.52%
	le	35.14%	36.55%	56.76%	57.02%	37.84%	34.21%
	les	45.95%	43.27%	67.57%	65.20%	43.24%	43.86%
	WORD 1	59.46%	64.33%	70.27%	70.18%	51.35%	43.57%
	WORD 2	45.95%	39.77%	45.95%	51.46%	48.65%	35.09%
	WORD 3	56.76%	59.06%	64.86%	76.32%	54.05%	53.22%
	SENT	40.54%	37.13%	35.14%	48.83%	45.95%	45.03%

are noted to have been achieved in the LPC features values of the kinematics, in addition to sharing the "SENT" task, but for healthy people with the SVM machine learning (ACC = 81.58%; AUC = 92.78%) and unhealthy people with the NN machine learning (ACC = 75.68%; AUC = 78.36%).

Key Observations

The superior performance of SVM classifiers compared to CNNs can be attributed to two main factors. Firstly, the sample sizes (~ 400 individuals) are relatively small for training deep learning models effectively, which can lead to overfitting in CNNs. Secondly, the handwriting dynamics captured here are better represented as sequential signals rather than spatial images, favoring the temporal modeling strengths of kernel-based classifiers like SVMs.

Overall, the SVM classifiers consistently achieved the highest accuracy across tasks compared to NN and CNN models, particularly in tasks involving longer handwriting sequences (e.g., "SENT" and "SG"). Robotic augmentation of features notably enhanced classification performance, especially in distinguishing gender differences in individuals affected by Parkinson's disease. The best result was obtained on the "SENT" task with an accuracy (ACC) of 81.58% and AUC of 92.78% in healthy individuals, demonstrating the robustness of the proposed method.

Analysis of Handwriting in Healthy and Unhealthy People by Gender with Raw Wacom Output

In this section, we present a new experiment designed to evaluate the impact of our robotic features on classification accuracy. We compare the performance obtained with raw data from the pen tablet versus data generated using robotic features. For raw Wacom data, we refer to the tuple (x,y,p).

Specifically, Table 12 shows that the best accuracy with BiosecurID was 59.90% and in PaHaW was 63.89% in some specific tasks. The rest of the performances are below 54.00%. Using LPC, experimental results of the robotic features (kinematics, dynamics, or both) outperform these results, at over 75%, as we can see in Tables 3, 5, and 7.

Although SSA improved the performances in Table 13, especially in the case of WORD 1 in PaHaW, we observe better performances with robotic features in Tables 4, 6, and 8, achieving around 78% in ACC and 80% in AUC in this dataset. On the other hand, better performances were consistently obtained with BiosecurID with the proposed features.

In the case of gender classification in unhealthy individuals, higher confusion is observed in Table 14 with results of around 50%. SSA features slightly improved these results as shown in Table 15. Although Tables 9, 10, and 11 also reflect high confusion in these tasks, better

Table 12 Classification accuracy (ACC) and area under the curve (AUC) for LPC raw data features in healthy handwriting samples using SVM, NN, and CNN classifiers

Database	Handwriting task	SVM		NN		CNN	
		ACC	AUC	ACC	AUC	ACC	AUC
BiosecurID	HW1	59.90%	65.79%	59.90%	63.35%	51.52%	45.54%
	HW2	54.00%	54.86%	52.25%	53.75%	48.75%	52.31%
	HW3	53.55%	0.00%	53.05%	47.80%	53.55%	44.63%
	SG	53.87%	12.97%	53.06%	46.35%	53.81%	48.79%
	SG FAKE	53.67%	49.91%	53.01%	47.43%	53.67%	44.52%
PaHaW	SPIRAL	52.78%	5.26%	50.00%	38.39%	63.89%	61.61%
	l	52.63%	5.00%	44.74%	35.28%	47.37%	46.39%
	le	52.63%	5.00%	44.74%	33.06%	52.63%	48.06%
	les	52.63%	5.00%	52.63%	40.56%	52.63%	46.11%
	WORD 1	52.63%	5.00%	39.47%	37.78%	42.11%	41.67%
	WORD 2	52.63%	5.00%	39.47%	43.61%	55.26%	56.11%
	WORD 3	52.63%	5.00%	55.26%	40.28%	52.63%	55.83%
	SENT	52.63%	5.00%	31.58%	35.56%	39.47%	38.33%

Table 13 Classification accuracy (ACC) and area under the curve (AUC) for SSA raw data features in healthy handwriting samples using SVM, NN, and CNN classifiers

Database	Handwriting task	SVM		NN		CNN	
		ACC	AUC	ACC	AUC	ACC	AUC
BiosecurID	HW1	62.94%	67.42%	63.45%	66.17%	49.75%	48.75%
	HW2	56.75%	60.17%	53.50%	56.68%	50.25%	47.39%
	HW3	65.23%	68.33%	62.18%	65.60%	52.79%	52.23%
	SG	66.75%	70.90%	67.87%	73.95%	49.63%	48.80%
	SG FAKE	58.68%	60.70%	57.93%	61.05%	48.83%	48.04%
PaHaW	SPIRAL	52.78%	52.94%	44.44%	59.75%	50.00%	45.20%
	l	68.42%	77.22%	60.53%	76.39%	60.53%	65.28%
	le	42.11%	53.61%	52.63%	61.67%	44.74%	29.72%
	les	52.63%	53.06%	55.26%	66.39%	44.74%	40.56%
	WORD 1	47.37%	50.28%	44.74%	50.83%	47.37%	42.78%
	WORD 2	57.89%	73.06%	52.63%	60.83%	42.11%	41.39%
	WORD 3	52.63%	53.33%	55.26%	58.33%	44.74%	45.28%
	SENT	60.53%	56.94%	47.37%	50.83%	50.00%	50.83%

Table 14 Classification accuracy (ACC) and area under the curve (AUC) for LPC raw data features in unhealthy handwriting samples using SVM, NN, and CNN classifiers

Database	Handwriting task	SVM		NN		CNN	
		ACC	AUC	ACC	AUC	ACC	AUC
PaHaW	SPIRAL	0.00%	0.00%	44.44%	36.73%	44.44%	40.43%
	l	51.35%	52.78%	35.14%	34.50%	40.54%	25.44%
	le	51.35%	52.78%	54.05%	44.15%	43.24%	35.96%
	les	51.35%	52.78%	40.54%	47.95%	51.35%	54.97%
	WORD 1	51.35%	52.78%	35.14%	38.01%	51.35%	47.66%
	WORD 2	51.35%	47.22%	37.84%	30.41%	45.95%	34.50%
	WORD 3	51.35%	52.78%	40.54%	41.81%	54.05%	41.52%
	SENT	51.35%	52.78%	54.05%	53.22%	59.46%	48.83%

Table 15 Classification accuracy (ACC) and area under the curve (AUC) for SSA raw data features in unhealthy handwriting samples using SVM, NN, and CNN classifiers

Database	Handwriting task	SVM		NN		CNN	
		ACC	AUC	ACC	AUC	ACC	AUC
PaHaW	SPIRAL	58.33%	70.37%	41.67%	40.43%	38.89%	54.32%
	l	78.38%	77.49%	59.46%	65.79%	56.76%	52.92%
	le	40.54%	48.54%	43.24%	51.56%	43.24%	35.67%
	les	51.35%	58.48%	56.76%	64.33%	45.95%	43.27%
	WORD 1	48.65%	63.16%	54.05%	59.06%	51.35%	37.13%
	WORD 2	40.54%	40.35%	59.46%	54.39%	48.65%	40.06%
	WORD 3	32.43%	42.11%	48.65%	49.12%	51.35%	57.02%
	SENT	56.76%	59.65%	59.46%	59.06%	51.35%	59.06%

performances are shown with robotic features, especially with kinematic features, obtaining performances of over 75%.

Conclusions

A deeper analysis of the extracted kinematic and dynamic features could enable the identification of biomechanical signatures distinguishing gender and pathology. For example, torque patterns may reveal reduced wrist mobility in Parkinson's disease, or greater finger agility in female writers. Future work will focus on interpretable models linking specific joint dynamics to motor strategies.

The development of a robotic model for gender-based motion analysis has proven highly effective in replicating and analyzing handwriting movements in both healthy individuals and people with Parkinson's disease. This model offers essential quantitative insights into biomechanical variables, enabling precise and consistent assessments of kinematic and dynamic handwriting features.

Our findings reveal significant differences in handwriting between genders, with kinematic features achieving notable accuracy (ACC = 81.58%) and area under the curve (AUC = 92.78%) in the "Sent" task for healthy subjects. Additionally, SSA coefficients produced strong results in the "l" task (ACC = 76.32%, AUC = 89.44%). Compared to existing handwriting-based gender classification methods, our best accuracy of 81.58% outperforms previously reported rates, which typically range between 65 and 75%, as noted in [7, 20], and [35]. However, it is important to note that a direct comparison is limited by differences in datasets, writing tasks, and experimental setups. Moreover, the referenced studies primarily involve healthy individuals, whereas our work also considers participants with Parkinson's disease, adding further complexity to the comparison. These outcomes, derived from the PaHaW database using SVM classifiers, underline the robustness of the proposed methodology.

For individuals with Parkinson's disease, the spiral task achieved an ACC of 75.00% and an AUC of 70.37% with SVM, demonstrating the efficacy of dynamic data in gender classification among neurodegenerative populations.

These findings advance our understanding of how cognitive and neuromotor processes influence handwriting, providing a bioinspired approach to diagnosing neurological conditions and enhancing biometric identification. The use of robotic systems that emulate human arm dynamics highlights the potential for future cognitive biometric tools capable of monitoring subtle cognitive-motor changes over time.

The implications of this work extend beyond handwriting analysis. Firstly, it underscores the importance of bioinspired cognitive computation in addressing broader challenges in human–computer interaction and neurodiagnostics. Secondly, it highlights a pathway for integrating cognitive modeling and robotics to enhance e-Health applications, such as early detection of neurodegenerative diseases, including Parkinson's. Finally, it opens avenues for further research into gender-based cognitive differences and their manifestations in motor tasks.

Beyond gender classification, the proposed robotic modeling framework holds potential for broader applications such as motor rehabilitation, handwriting synthesis for assistive technologies, and cognitive-motor skill assessment. By simulating and perturbing motor parameters, it could serve as a platform to study learning dynamics, error recovery, and adaptation in handwriting.

Future studies should aim to expand the dataset to include other neurodegenerative diseases and investigate additional cognitive features, such as handwriting task complexity and error patterns, to refine the model's predictive capacity. Additionally, integrating supplementary biosensors, such as electroencephalography (EEG) or electromyography (EMG), could provide a more comprehensive understanding of the cognitive-motor interface.

Limitations and Future Work

While the presented approach shows promising results, several limitations must be acknowledged. Firstly, the handwriting datasets used are limited in size and diversity, which may

introduce biases based on language, writing style, or cultural background. Secondly, the CNN model comprised a shallow neural network composed of fully connected layers with 64 and 32 neurons, using ReLU activations, which is appropriate for the low-dimensional, non-image input features used in this study. Due to the lack of pretrained CNNs for handwriting time signals, transfer learning was not employed. Future work could explore this avenue. Thirdly, the robotic model is based on average anthropometric parameters and fixed wrist postures, which may not perfectly reflect individual variability. Fourthly, the generalization to other scripts (e.g., Arabic, Cyrillic) remains unexplored. Future work will address these issues by incorporating larger, more diverse datasets, modeling variable wrist configurations, and exploring multilingual handwriting samples.

Author Contribution Belen Esther Aleman: Data curation, Investigation, Writing – original draft. Moises Diaz: Writing – review & editing, Funding acquisition, Formal analysis. Miguel A. Ferrer: Supervision, Investigation, Conceptualization. Jose Juan Quintana: Visualization, Methodology, Validation. Marcos Faundez-Zanuy: Writing – review & editing, Supervision, Funding acquisition.

Funding Open Access funding provided thanks to the CRUE-CSIC agreement with Springer Nature. This research was partly supported by PID2023-146620OB-I00 and PID2023-146644OB-I00, funded by the Spanish Ministry of Science, Innovation and Universities/State Research Agency (MICIU/AEI)https://doi.org/10.13039/501100011033and the European Union's ERDF program.

Data Availability The raw data BiosecurID and PaHaW were presented in [21] and [17], respectively, and are available from the authors of those papers.

The authors declare no competing interests.

Declarations

Competing interests The authors declare that they have no conflicts of interest.

All procedures performed in studies involving human participants were in accordance with the ethical standards of the institutional and/or national research committee and with the 1964 Declaration of Helsinki and its later amendments or comparable ethical standards. For this type of study, formal consent is not required.
This chapter does not contain any studies with animals performed by any of the authors.

References

1. Al Maadeed S, Hassaine A. Automatic prediction of age, gender, and nationality in offline handwriting. EURASIP J Image Video Process. 2014;2014:1–10.
2. AL-Qawasmeh N, Suen CY. Gender detection from handwritten documents using concept of transfer-learning. In: International conference on pattern recognition and artificial intelligence. Cham: Springer International Publishing; 2020. p. 3–13.
3. Alzubaidi L, Zhang J, Humaidi AJ, Al-Dujaili A, Duan Y, Al-Shamma O, Santamaría J, Fadhel MA, Al-Amidie M, Farhan L. Review of deep learning: concepts, CNN architectures, challenges, applications, future directions. Journal of big Data. 2021Dec;8:1–74.
4. Asci F, Scardapane S, Zampogna A, D'Onofrio V, Testa L, Patera M, et al. Handwriting declines with human aging: a machine learning study. Front Aging Neurosci. 2022;14: 889930.
5. Benjumea AC. Datos antropométricos de la población laboral española. Prevención, trabajo y salud: Revista del Instituto Nacional de Seguridad e Higiene en el Trabajo. 2001;14:22–30.
6. Bowers AJ, Zhou X. Receiver operating characteristic (ROC) area under the curve (AUC): a diagnostic measure for evaluating the accuracy of predictors of education outcomes. Journal of Education for Students Placed at Risk (JESPAR). 2019Jan 2;24(1):20–46.
7. Bouadjenek N, Nemmour H, Age CY, gender and handedness prediction from handwriting using gradient features. In,. 13th international conference on document analysis and recognition (ICDAR). IEEE. 2015;2015:1116–20.
8. Bradbury J. Linear predictive coding. McG. Hill. 2000 Dec 5.
9. Cawley GC, Talbot NL. Fast exact leave-one-out cross-validation of sparse least-squares support vector machines. Neural Netw. 2004;17(10):1467–75.
10. Choi RY, Coyner AS, Kalpathy-Cramer J, Chiang MF, Campbell JP. Introduction to machine learning, neural networks, and deep learning. Transl Vis Sci Technol. 2020Jan 28;9(2):14.
11. Cordasco G, Buonanno M, Faundez-Zanuy M, Riviello MT, Likforman-Sulem L, Esposito A. Gender identification through handwriting: an online approach. In: 2020 11th IEEE International Conference on Cognitive Infocommunications (CogInfoCom). IEEE; 2020. p. 000197–202.
12. Craig, J. Introduction to robotics: mechanics and control 4th edition, Pearson education, 2017, ISBN: 978–0133489798
13. Denavit J, Hartenberg RS. A kinematic notation for lower-pair mechanisms based on matrices. J Appl Mech. 1955;22(2):215–21.
14. Diaz, M, Ferrer, MA and Quintana, JJ, (2018a), August. Robotic arm motion for verifying signatures. In: 2018 16th International conference on frontiers in handwriting recognition (ICFHR) (pp. 157–162). IEEE.
15. Diaz M, Ferrer MA, Quintana JJ. (2018b) Anthropomorphic features for on-line signatures. IEEE Trans Pattern Anal Mach Intell. 2018;41(12):2807–19.
16. Diaz M, Ferrer MA, Quintana JJ, Wolniakowski A, Trochimczuk R, Miatliuk K, Castellano G, Vessio G. Neural network modelling of kinematic and dynamic features for signature verification. Pattern Recogn Lett. 2025;187:130–6.
17. Drotár P, Mekyska J, Rektorová I, Masarová L, Smékal Z, Faundez-Zanuy M. Evaluation of handwriting kinematics and pressure for differential diagnosis of Parkinson's disease. Artif Intell Med. 2016Feb;1(67):39–46.
18. Drotár P, Mekyska J, Rektorová I, Masarová L, Smékal Z, Faundez-Zanuy M. Analysis of in-air movement in handwriting: a novel marker for Parkinson's disease. Comput Methods Programs Biomed. 2014;117(3):405–11.
19. Faundez-Zanuy M, Brotons-Rufes O, Paul-Recarens C, Plamondon R. On handwriting pressure normalization for

interoperability of different acquisition stylus. IEEE Access. 2021Jan;21(9):18443–53.
20. Faundez-Zanuy M, Mekyska J. Analysis of gender differences in online handwriting signals for enhancing e-Health and e-Security applications. Cogn Comput. 2023;15(1):208–19.
21. Fierrez J, Galbally J, Ortega-Garcia J, Freire MR, Alonso-Fernandez F, Ramos D, Gracia-Roche JJ. BiosecurID: a multimodal biometric database. Pattern Anal Appl. 2010;13:235–46.
22. Hassani H. Singular spectrum analysis: methodology and comparison. Journal of Data Science, 5, 239–257.
23. Høifødt H. Dynamic modeling and simulation of robot manipulators: the Newton-Euler formulation [Master's thesis]. Institutt for teknisk kybernetikk; 2011.
24. Lagarias JC, Reeds JA, Wright MH, Wright PE. Convergence properties of the Nelder-Mead simplex method in low dimensions. SIAM J Optim. 1998;9(1):112–47.
25. Lavazza L, Morasca S, Rotoloni G. On the reliability of the area under the ROC curve in empirical software engineering. In: Proceedings of the 27th International Conference on Evaluation and Assessment in Software Engineering. 2023 Jun 14. p. 93–100.
26. Levi G, Hassner T. Age and gender classification using convolutional neural networks. In: Proceedings of the IEEE conference on computer vision and pattern recognition workshops. 2015. p. 34–42.
27. Mahesh B. Machine learning algorithms-a review. Int J Sci Res (IJSR). 2020Jan;9(1):381–6.
28. Manor LK. Analysis of upper limb prosthetic and BMI data in Atlantic Canada. New Brunswick, Canada: University of New Brunswick; 2014.
29. Marzinotto G, Rosales JC, El-Yacoubi MA, Garcia-Salicetti S. Age and gender characterization through a two layer clustering of online handwriting. In: Advanced concepts for intelligent vision systems: 16th international conference, ACIVS 2015, Catania, Italy, October 26–29, 2015. Proceedings 16. Springer International Publishing; 2015. p. 428–39.
30. Maurer MN. Correlates of early handwriting: differential patterns for girls and boys. Early Educ Dev. 2024;35(4):843–58.
31. Palaiahnakote S, Kaljahi MA, Kanchan S, Pal U, Lopresti D, Lu T. A robust script independent handwriting system for gender identification. Expert Syst Appl. 2024;249: 123576.
32. Qawaqneh Z, Mallouh AA, Barkana BD. Age and gender classification from speech and face images by jointly fine-tuned deep neural networks. Expert Syst Appl. 2017;85:76–86.
33. Rabaev I, Alkoran I, Wattad O, Litvak M. Automatic gender and age classification from offline handwriting with bilinear ResNet. Sensors. 2022;22(24):9650.
34. Russel NS, Selvaraj A. Gender discrimination, age group classification and carried object recognition from gait energy image using fusion of parallel convolutional neural network. IET Image Process. 2021;15(1):239–51.
35. Sesa-Nogueras E, Faundez-Zanuy M, Roure-Alcobé J. Gender classification by means of online uppercase handwriting: a text-dependent allographic approach. Cogn Comput. 2016;8:15–29.
36. Shin J, Uchida Y, Maniruzzaman M, Hirooka K, Megumi A, Yasumura A. Online handwriting-based gender recognition using statistical and machine learning approaches. IEEE Access. 2024.
37. Spratling MW. A review of predictive coding algorithms. Brain Cogn. 2017Mar;1(112):92–7.
38. Vehtari A, Gelman A, Gabry J. Practical Bayesian model evaluation using leave-one-out cross-validation and WAIC. Stat Comput. 2017;27:1413–32.